Design, Molecular Docking, Synthesis, and Pharmacological Evaluation of Nabumetone-Derived Oxadiazole and Thiadiazole Schiff Bases as Potential EGFR Inhibitors for NSCLC

Ahmed Haloob Kadhim*, Monther Faisal Mahdi*, Ayad M.R. Raauf**
Department of Pharmaceutical Chemistry, College of Pharmacy, Mustansiriyah University, Baghdad, Iraq
****College of Pharmacy, Al-Farahidi University, Baghdad, Iraq***

Article Info:

Received 29 Apr 2025
Revised 25 May 2025
Accepted 23 June 2025
Published 31 Dec 2025
Corresponding Author email:
ahmed_haloub@uomustansiriyah.edu.iq
Orcid: https://orcid.org/0009-0008-1463-1782

DOI: https://doi.org/10.32947/ajps.v25i5.1318

Abstract:

Lung cancer is the leading cause of cancer-related mortality globally, with non-small cell lung cancer (NSCLC) making up about 85%. Overexpression or mutation of the epidermal growth factor receptor (EGFR) drives tumor proliferation in NSCLC. Although first-generation EGFR tyrosine kinase inhibitors (TKIs) like gefitinib and erlotinib showing a rapid acquired resistance, often via the T790M mutation, limits their long-term effectiveness.

This study synthesized two new nabumetone-based Schiff base derivatives with either a 1,3,4-oxadiazole ring (compounds 5a-c) or a 1,3,4-thiadiazole ring (compounds 6a-e). Characterization was conducted via FT-IR and NMR spectroscopy, and *In vitro* cytotoxicity assays using the MTT method were conducted on A549 non-small cell lung cancer (NSCLC) cells at different time intervals (e.g., 24 and 48 hours) to evaluate the antiproliferative effect. The 1,3,4-thiadiazole series (6a-e) was more potent than the oxadiazoles (5a-c), with compounds 6b and 6e showing the lowest 48-hour IC_{50} values (~40.9 µM and ~30.2 µM, respectively), outperforming erlotinib (IC_{50} ~51.3 µM). These results suggest that thiadiazole sulfur substituents (e.g., 6b, 6e) enhance anticancer activity through stronger interactions. This work introduces new nabumetone-derived compounds with promising antiproliferative activity against NSCLC, identifying compounds 6b and 6e as potent lead candidates for further in vivo and pharmacokinetic evaluation to advance EGFR-targeted cancer therapies. Molecular docking investigations further validated these results, demonstrating that all compounds have stronger interactions within the EGFR binding pocket, achieving superior PLP fitness scores range from 90.61 to 78.46 compared to erlotinib 77.62. These computational findings support the experimental data, indicating the promising potential of these derivatives as EGFR inhibitors.

Keywords: Non-small cell lung cancer; Epidermal growth factor receptor; 1,3,4-Oxadiazole; 1,3,4-Thiadiazole; Schiff base; Cytotoxicity Assay

تصميم وإرساء جزيئي وتخليق وتقييم دوائي لقواعد شيف المحتوية على أوكساديازول وثايا ديازول والمشتقة من النابوميتون كمثبطات محتملة لمستقبل عامل النمو البشري (EGFR) لعلاج سرطان الرئة غير صغير الخلايا (NSCLC)

أحمد حالوب كاظم*، منذر فيصل مهدي*، أياد محمد رؤوف**
قسم الكيمياء الصيدلانية، كلية الصيدلة، الجامعة المستنصرية، بغداد، العراق
****كلية الصيدلة، جامعة الفراهيدي، بغداد، العراق***

الخلاصة:
يُعد سرطان الرئة السبب الأول للوفيات المرتبطة بالسرطان على مستوى العالم، حيث يشكّل سرطان الرئة غير صغير الخلايا (NSCLC) نحو 85% من الحالات. يرتبط الإفراط في التعبير أو الطفرات في مستقبل عامل النمو البشري (EGFR)بزيادة تكاثر الأورام في سرطان الرئة غير صغير الخلايا. وعلى الرغم من النجاح الأولي لمثبطات التيروزين كيناز (TKIs) من الجيل الأول مثل الجيفيتينيب والإرلوتينيب، إلا أن تطور المقاومة المكتسبة، وغالبًا عبر طفرةT790M ، حدّ من فعاليتها على المدى الطويل. في هذه الدراسة، تم تخليق مشتقات جديدة من قواعد شيف المعتمدة على النابوميتون، تضمنت حلقة 1,3,4-أوكساديازول (5a-c) أو حلقة 1,3,4-ثايا-ديازول (6a-e). وقد تم توصيف المركبات باستخدام تقنيات مطيافية الأشعة تحت الحمراء (FT-IR) والرنين المغناطيسي النووي(NMR) ، كما تم إجراء اختبارات السمية الخلوية باستخدام اختبار MTT في المختبر على خلايا A549 لسرطان الرئة غير صغير الخلايا (NSCLC) عبر فترات زمنية مختلفة (مثل 24 و48 ساعة) لتقييم التأثير المضاد للتكاثر. وأظهرت النتائج تأثيراً مضاداً للتكاثر يعتمد على التركيز والزمن. أظهرت سلسلة مركبات الثايا-ديازول (6a-e) نشاطاً أعلى مقارنة بسلسلة الأوكساديازول(5a-c) ، حيث أظهر المركبان 6b و6e أقل قيم IC50 بعد 48 ساعة (حوالي 40.9 و30.2 ميكرومول على التوالي)، متفوقين بذلك على الإرلوتينيب (IC50 ≈ 51.3 ميكرومول) كما في المركبين 6b و 6e) قد يعزز النشاط المضاد للسرطان من خلال تعزيز التفاعلات الحيوية مع المستقبل. توضح هذه الدراسة إمكانية استخدام هذه المشتقات الجديدة المعتمدة على النابوميتون كمثبطات واعدة لمستقبلEGFR ، مع إبراز المركبين 6b و 6e كمرشحين رئيسيين لمزيد من التقييمات داخل الجسم الحي والدراسات الحركية الدوائية بهدف تطوير علاجات فعالة تستهدف مستقبلات EGFR في علاج السرطان. وكما أكدت دراسات الارساء الجزيئي صحة هذه النتائج، حيث أظهرت أن جميع المركبات تمتلك تفاعلات أقوى داخل موقع الارتباط الخاص بمستقبل EGFR، محققة درجات ملاءمة PLP أعلى تراوحت بين 90.61 و78.46، مقارنةً بالإرلوتينيب الذي سجل 77.62. تدعم هذه النتائج الحاسوبية البيانات التجريبية، مما يشير إلى الإمكانية الواعدة لهذه المشتقات كمثبطات لمستقبل EGFR.

الكلمات المفتاحية :سرطان الرئة غير صغير الخلايا؛ مستقبل عامل النمو البشري؛ 1,3,4-أوكساديازول؛ 1,3,4-ثايا-ديازول؛ قاعدة شيف؛ اختبار السمية الخلوية.

1. Introduction

Lung cancer ranks as the highest cause of death from any malignancy, with a staggering 2 million new cases detected and 1.8 million lives claimed in the year 2018 [1]. Suppose the diagnosis is done early (i.e., Stage I-II). In that case, the survival rate becomes around 56% [2]. The prognosis improves significantly when lung cancer is detected in its early stages. However, the low percentage of early diagnoses stands at just 16% [3].

Significant research has focused on tyrosine kinases (TKs), which are implicated in nearly all cancers. TKs play a crucial role in all cancer development stages. The discovery of protein-tyrosine kinase (PTK) and nonreceptor tyrosine kinase (NRTK) has been vital in cancer research development.[4] EGFR mutations primarily drive most NSCLC cases. Treatment strategies shifted to protein kinase inhibitors targeting this protein. Gefitinib, the first EGFR inhibitor, received FDA approval in 2003 for lung cancer with activating EGFR mutations [5]. The FDA authorized Erlotinib for first-line therapy in metastatic NSCLC cases that led to the development of a mutation (EGFR-exon 19 deletions and L858R mutations) [6, 7]. Because both drugs interact with the THR790 residue, a mutation at this site leads to resistance to these drugs [8]. With the development of third-generation TKIs, such as osimertinib and rociletinib, which have been designed to prevent the acquisition of resistance, without the side effects encountered during treatment with first- or second-generation TKIs. C797S mutations resistant to osimertinib occur in 10% of patients post-osimertinib administration [9].

Therefore, there is a continuous need to explore new scaffolds and molecular strategies to inhibit EGFR and combat resistant NSCLC. One approach to discovering novel anticancer agents is to modify existing drugs with known safety profiles to confer new activities.

Nitrogen-containing heterocycles are central to drug development, making up over 75% of FDA-approved drugs. Research design of numerous new heterocycles, many showing significant physiological properties for medicinal use applications [10]. The 1,3,4-oxadiazole is a five-membered heterocyclic structure with one oxygen and two nitrogen atoms at positions 1, 3, and 4, respectively—those with a significant interest in medicinal chemistry for its diverse pharmacological activities, especially its anticancer properties [11, 12].

Some 1,3,4-thiadiazole derivatives disrupt DNA replication. It seems 1,3,4-thiadiazole molecules inhibit human tumor and bacterial cell proliferation by interfering with DNA synthesis, resulting in growth inhibition. This has prompted a search for new antibiotics and anticancer drugs among their derivatives [13].

Nabumetone is an oral anti-inflammatory, known as 4-(6-methoxy-2-naphthyl) butane-2-one. Like other NSAIDs, it inhibits cyclooxygenase (COX-1 and COX-2), decreasing prostaglandin production, a key mediator of pain and swelling. As a pro-drug, *in vivo* anti-cyclo-oxygenase effects are activated after the liver metabolizes it to 6-methoxy-2-naphthylacetic acid (6-MNA). The drug has analgesic, antipyretic, and anti-inflammatory properties like other NSAIDs [14].

In structural drug design and computer-aided drug discovery, molecular docking is a key process. It is a computer-aided method for determining the correct binding position and pose of ligands in the active site of a protein. This allows the assessment of protein-ligand binding interactions in terms of estimating binding affinities to support the prediction on a compound's biological activity and SAR. It also provides value to the rational ligand design targeting on particular residues in the binding pocket with higher binding affinity.[15, 16]

We aimed to create novel nabumetone-based Schiff base derivatives with a 1,3,4-oxadiazole or 1,3,4-thiadiazole ring to assess their potential as EGFR inhibitors for NSCLC therapy. The nabumetone naphthyl butanone core is a versatile anchor for attaching heterocyclic moieties to synergize cytotoxic pharmacophores. We hypothesized that linking a 2-amino-1,3,4-oxadiazole or 2-amino-1,3,4-thiadiazole to nabumetone via an imine linkage could produce compounds that engage the EGFR kinase domain and inhibit NSCLC cell growth.

This study is aimed to synthesis the best set of compounds and identification of the synthesized compounds by FTIR, ^{13}C-NMR, and ^{1}H-NMR. And evaluate their EGFR binding via molecular docking, and assess antiproliferative activity against A549 cells.

The general structure of the proposed compounds, series one of 1,3,4-oxadiazole derivatives (5a-c), and series two of 1,3,4-thiadiazole derivatives (6a-e):

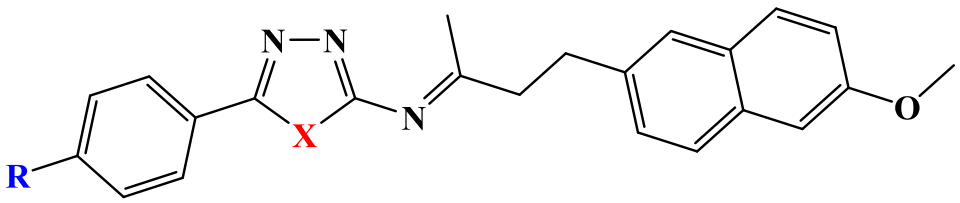

(5a-c, 6a-e)

X= O , S

R= H(a), Cl(b) , OCH_3(c),CH_3(d) , NO_2(e)

2. Materials and Methods

2.1. Molecular Docking Study

EGFR proteins were downloaded from the Protein Data Bank, specifically 4HJO, with a resolution of 2.75 Å, to initiate the docking process. This structure, 4HJO, represents the crystal structure of EGFR protein complexes with erlotinib. The protein structure was prepared by removing all water molecules, retaining only HOH 1104 due to its critical role in ligand stabilization, which is crucial for erlotinib activity by forming a bridge with THR 830 and THR 766. Hydrogen atoms were included to ensure the appropriate ionization and tautomeric states of amino acid residues. The ligand docking process was conducted utilizing GOLD software (Hermes 2022.3.0) from the Cambridge Crystallographic Data Centre (CCDC). Version with the full license used to prepare the receptor and make it ready for docking, as well as to obtain different poses for each compound.

The process of docking need the extraction of reference ligand (erlotinib), defined the binding site within the protein as the reference ligand with selection all atoms within 10 Å of the reference ligand in the protein structure to including in docking process for the binding site, set pose number to ten for each compound, set the template as chemscore_kinase, choosing a ChemPLP as fitness function (ChemPLP fitness refers to the "Piecewise Linear Potential" It is a scoring function used to evaluate the quality of ligand poses within a protein binding site during docking simulations, it used to predict ligand binding poses and rank compounds depend on interaction with protein, the PLP Fitness score is a sum of steric interaction score, hydrogen bonding score, ligand steric score and protein flexibility score), turn off allowing early termination, set the process to done in slow (most accurate), and then performed docking process to generate the result.

2.2. Chemicals and Instruments

Only the highest-purity chemicals have been acquired for synthesis purposes, all benzaldehyde derivatives including 4-chlorobenzaldehyde, 4-methoxybenzaldehyde, 4-methylbenzaldehyde, 4-nitrobenzaldehyde, as well as nabumetone, semicarbazide hydrochloride, and thiosemicarbazide were obtained from Sigma-Aldrich (Germany). Benzaldehyde was purchased from Alpha Chemical (India), while iodine and glacial acetic acid were sourced from LOBA CHEMIE and Himedia (India), respectively.

Instrumentation utilized in the characterization of synthesized compounds included a Bruker NMR spectrometer (USA) operating at 300 MHz for ^{1}H NMR and 75 MHz for ^{13}C NMR, a Shimadzu FTIR spectrophotometer model 8400S (Japan), and an electric melting point apparatus from Stuart (UK).

2.3 Chemical Synthesis Scheme

The synthesis of intermediate (1a-c,2a-e,3a-c,4a-e) and final compounds (5a-c, 6a-e) was done according to the following scheme (1).

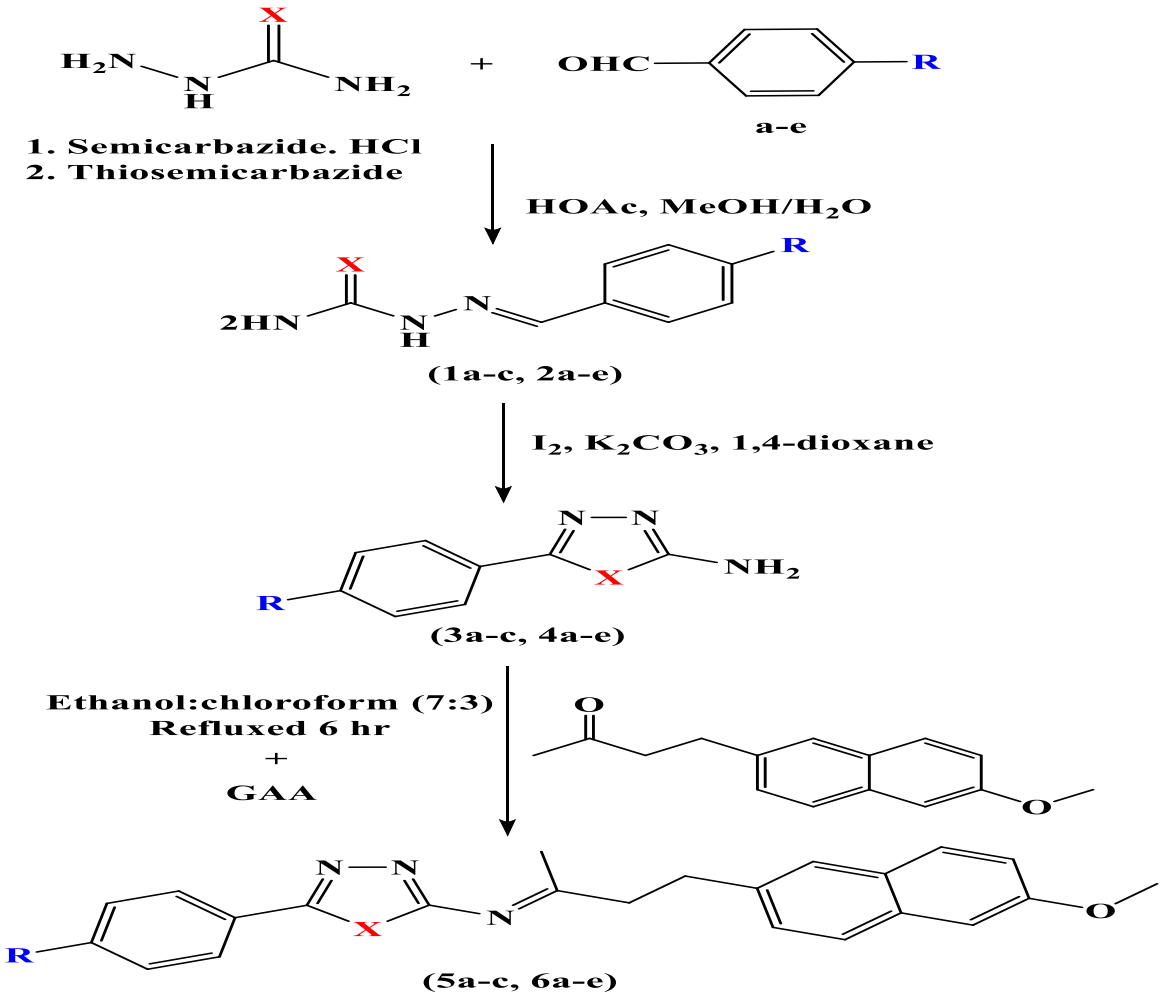

Scheme (1): Synthesis of the intermediate and the final compounds.

Step 1: General Procedure for the Synthesis of hydrazine-1-carboxamide (1a-c) and hydrazine-1-carbothioamide derivatives (2a-e)

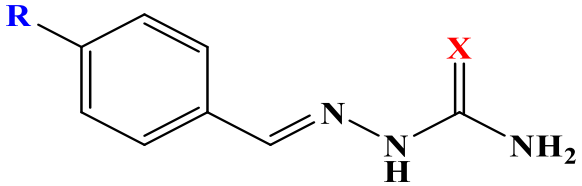

(1a-c) and (2a-e)

X= O , S

R= H(a), Cl(b) , OCH_3(c),CH_3(d) , NO_2(e)

Equimolar amounts of semicarbazide HCl (1 mmol) and sodium acetate (1 mmol) were mixed in water. Solutions of the benzaldehyde [benzaldehyde (a), 4-chlrobenzaldehyde (b) and 4-methoxy benzaldehyde (c)] (1 mmol) in methanol were added separately dropwise with stirring at room temperature for 1 hr, the precipitates were filtered, washed with cold water, and dried to yield intermediates hydrazine-1-carboxamide derivatives (1a-c).

Similarly, thiosemicarbazones (2a-e) were obtained by reacting thiosemicarbazide (1 mmol) with the appropriate benzaldehyde [benzaldehyde (a), 4-chlrobenzaldehyde (b) and 4-methoxy benzaldehyde (c), 4-methylbenzaldehyde (d) and 4-nitrobenzaldehyde (e)] (1 mmol) in a 1:1 methanol-water mixture, catalyzed by few drops of glacial acetic acid and stirred at room temperature for 1 hr. The solid product were filtered and dried [17].

Step 2: General Procedure for Synthesis of 1,3,4-oxadiazol-2-amine (3a-c) and 1,3,4-thiadiazol-2-amine derivatives (4a-e)

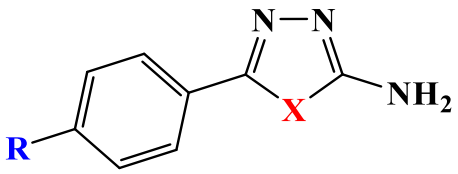

(3a-c) and (4a-e)

X= O , S

R= H(a), Cl(b) , OCH_3(c),CH_3(d) , NO_2(e)

(1 mmol) of the semicarbazones (1a-c) or thiosemicarbazones (2a-e) were dissolved in 10 mL of 1,4-dioxane, then three mmol of potassium carbonate and 1.2 mmol of iodine were added. The mixtures were stirred at 80°C for 4 hours. After cooling, add 40 mL of 5% sodium thiosulfate solution to eliminate excess iodine. The products were extracted with dichloromethane: methanol (10:1) to afford pure compounds (3a-c) or (4a-e) [17].

Step 3: General Procedure for the Synthesis of Final Compounds (5a-c and 6a-e)

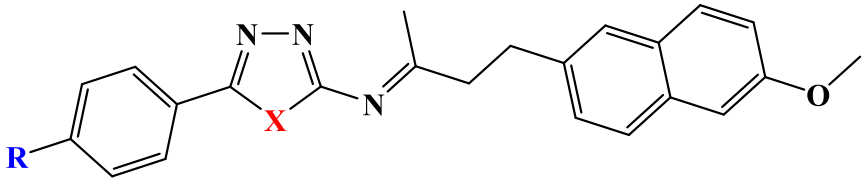

(5a-c, 6a-e)

X= O , S

R= H(a), Cl(b) , OCH_3(c),CH_3(d) , NO_2(e)

In a 100 mL round-bottom flask, (1 mmol) of the compounds 3a-c or 4a-e was combined with (1 mmol) of nabumetone (0.212 g) in an ethanol: chloroform (7:3, 50 mL). Subsequently, glacial acetic acid (1 mL) was introduced as a catalyst. Reflux for 6 hours

while being stirred continuously. Evaporated at reduced pressure, the precipitate was recrystallized in ethanol to produce the pure final Schiff base derivatives (5a-c and 6a-e) [18].

2.4 Cytotoxicity Assay

The MTT assay on a human NSCLC cell line (A549) evaluated the antiproliferative effects of the final compounds. Cells were maintained in RPMI-1640 medium with 10% fetal bovine serum and 1% penicillin/streptomycin at 37°C in a humidified 5% CO_2 incubator. For the cytotoxicity assay, cells were plated in 96-well plates at approximately 8×103 cells per well and left to adhere overnight. Stock solutions of each test compound (5a-c, 6a-e) were dissolved in DMSO (10 mM) and diluted in culture medium to the appropriate concentrations (with final DMSO <0.5%). Erlotinib was a positive control (reference drug), while untreated cells with 0.5% DMSO acted as a negative control. Each compound was tested in triplicate wells across a concentration range of 2 to 1000 µM. Following 48 hours of treatment, 20 µL of MTT reagent (5 mg/mL in PBS) was added to wells; the plates were incubated for 4 hr to form a formazan crystal and by using of 100 µL DMSO to dissolve the crystals, and by use microplate reader to measure the absorbance at 570 nm. Cell viability was computed as a percentage of the control (untreated) absorbance. Dose-response curves were plotted, and each compound's half-maximal inhibitory concentration (IC_{50}) values at 48 hours were computed via nonlinear regression analysis with GraphPad Prism (variable slope sigmoidal fit). Each IC_{50} value represents the mean from at least three independent experiments. A one-way ANOVA was conducted with a post-hoc Tukey test to analyze differences between compounds and the control drug, considering $p<0.05$ statistically significant.

3. Results and Discussion

3.1. Interpretation of Molecular Docking Study

Docking Results Virtual screening (VS) uses computer software to find compounds based on their fitting to the target receptor. The docking result determines the hydrogen bonds and the short contact distances between protein atoms and ligands. The high number of Hydrogen bond interactions and hydrophobic interactions increases the pharmacological activity required for substrate binding to the active site. [19, 20]

Molecular docking studies were conducted to assess the binding affinities and interaction profiles of the synthesized Schiff base derivatives (5a-c and 6a-e) against the EGFR receptor (PDB ID: 4HJO) using GOLD software. The ChemPLP fitness scores for the designed ligands ranged from 78.46 to 90.61, with compound 5a achieving the highest score (90.61), followed by 5c (86.65) and 5b (85.45), all surpassing the reference drug erlotinib, which scored 77.62. The high scores are attributed to favorable orientations and strong interactions within the binding pocket, particularly involving hydrogen bonds with key residues THR830 and THR766, often bridged by a conserved water molecule HOH 1104, as well as hydrophobic contacts with VAL702, MET742, LEU820, and LYS721. While the 1,3,4-oxadiazole derivatives (5a-c) generally showed stronger binding scores, the 1,3,4-thiadiazole compounds (6a-e) presented lower, yet significant, binding values between 78.46 and 80.91, supported by consistent hydrogen bonding and hydrophobic interactions with critical active-site residues. Erlotinib also interacted via hydrogen bonding with THR830 and THR766, demonstrating a similar binding mode to the newly synthesized compounds. The interactions of 5a, 5b, and erlotinib are depicted in table 1 and 2, providing representative visualizations of the ligand–receptor complexes. These

results underscore the potential of oxadiazole and thiadiazole scaffolds in enhancing EGFR binding and guide future design of potent EGFR inhibitors.

Table (1): Shows the Key interactions of all proposed compounds and reference compound erlotinib against EGFR (PDB: 4HJO) using GOLD software.

No.	Ligand Name	PLPfitness (Average Values)	H-bond interactions	Hydrophobic interactions
1	5a	90.61	Oxygen of oxadiazole with THR830 and Nitrogen of Imine with HOH 1104 bridges to THR830 and THR766	VAL702, MET742, LEU820 (2), THR830, Nitrogen of Imine with HOH 1104 bridges to THR830 and THR766
2	5b	85.45	Oxygen of oxadiazol ring with HOH 1104 bridges to THR830 and THR766	LEU768, LEU820, VAL702 (3), LYS721 (3), MET742, oxygen and carbon of oxadiazol ring from two bonds with HOH 1104 bridges to THR830 and THR766
3	5c	86.65	Oxygen of oxadiazol ring with THR830 and HOH1104 bridge with THR830 and THR766	MET742 (3), THR830 (2), and Oxygen of oxadiazol ring with HOH 1104 bridge to THR830 and THR766
4	6a	80.51	Two nitrogen atoms of the thiadiazole ring with THR830, and with HOH 1104 bridge to THR830 and THR766	MET742, THR830 (4), and VAL (7)
5	6b	80.91	Nitrogen of the thiadiazole ring with THR 830, and oxygen of the methoxy group with LYS704	LYS704, LEU694, LEU820, ASP831, LEU764 (4), VAL702, LEU753, and THR 830 (2)
6	6c	80.41	Oxygen of methoxy group with LYS704, Nitrogen of thiadiazol ring with LYS721	LYS704, LYS721, and VAL702
7	6d	80.36	HOH 1104 bridges between Nitrogen of the thiadiazol ring with THR 830 and THR 766	LEU764 (2), ASP831, LYS704, and LEU834
8	6e	78.46	Nitrogen of the thiadiazole ring with THR830 and HOH 1104 bridge to THR830 and THR766	LEU764, VAL702, LYS721, LEU694, Nitrogen of thiadiazole ring with THR830 and HOH 1104 bridge to THR830 and THR766
9	Erlotinib	77.62	Nitrogen of quinazoline ring with HOH 1104 bridge to THR830 and THR766	LEU834, GLY695, ALA719, LEU694 (3), VAL702, and Nitrogen of quinazoline ring with HOH 1104 bridge to THR830 and THR766

*Numbers in brackets refer to the number of bonds

Table (2): 3D intermolecular interactions of complexes between all proposed compounds and reference drug erlotinib with EGFR (PDB: 4HJO) using gold software.

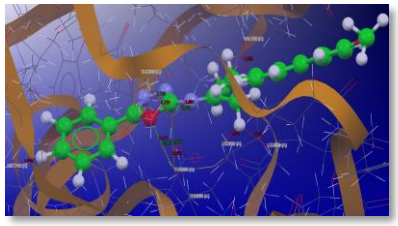 5a	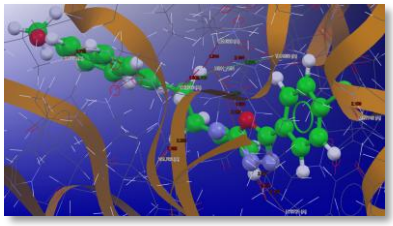 5b
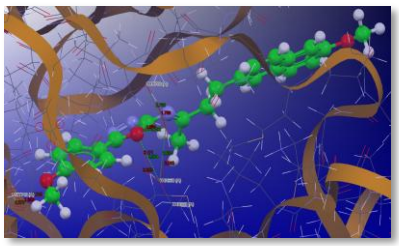 5c	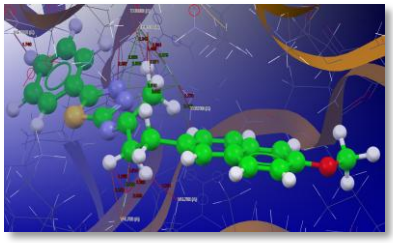 6a
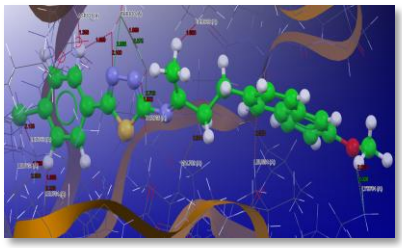 6b	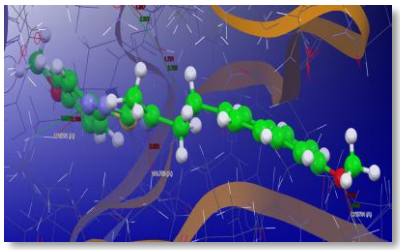 6c
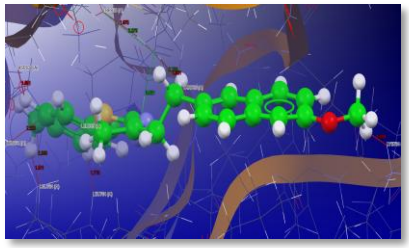 6d	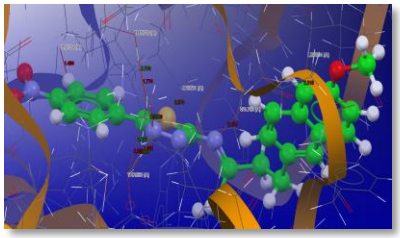 6e
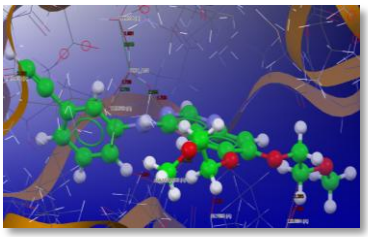 erlotinib	

Compounds are depicted as a stick and ball model. In contrast, the receptor is shown as a wireframe and ribbon; hydrogen bonds are illustrated with a green dashed line, while red dashed lines represent other short contacts.

3.2 Mechanism for the Formation of Intermediate Compounds (1a-c, 4a-e): Step 1: Schiff Base Formation (1a-c, 2a-e)

Semicarbazide hydrochloride (1) or thiosemicarbazide (2) react with benzaldehyde derivatives (a-e) to generate a Schiff bases or imine compounds. Imines are formed through a reversible reaction using acid-catalyzed conditions, which starts with the nucleophilic addition of the 1° amine from compounds (1) and (2) to the carbonyl group of benzaldehyde derivatives. This is followed by a proton transfer from nitrogen to oxygen, resulting in a neutral amino alcohol or carbinolamine. The carbinolamine's oxygen is then protonated by an acid catalyst, converting the -OH into a better leaving group (+OH_2). Loss of water leads to the formation of an iminium ion. The mechanism for the formation of the Schiff base is depicted in Scheme 2.[21]

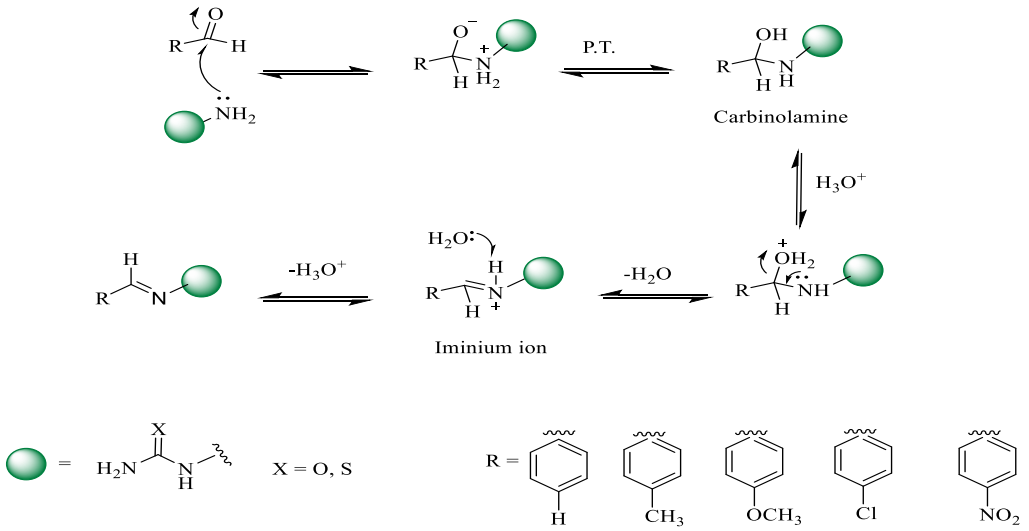

Scheme (2): Mechanism of formation of intermediates (1a-c and 2a-e). [22, 23]

The reaction was confirmed by the formation of (C=N) at (1581-1610 cm^{-1}) for the generated (1a-c) and (2a-e).

Step 2: Formation of 2-amino-1,3,4-oxadiazole (3a-c) and 2-amino-1,3,4-thiadiazole (4a-e)

Then, by adding potassium carbonate and iodine, the compounds 2-amino-1,3,4-oxadiazole (3a-c) and 2-amino-1,3,4-thiadiazole (4a-e) were formed.

The first reaction of I_2 with imine creates the α-iodo imine. This oxidative iodination, facilitated by K_2CO_3, could contribute to the selective cyclization of intermediate (A). As a result, the product is formed through consecutive SN_2-cyclization reactions and aromatization reactions A, as shown in Scheme 3 [21].

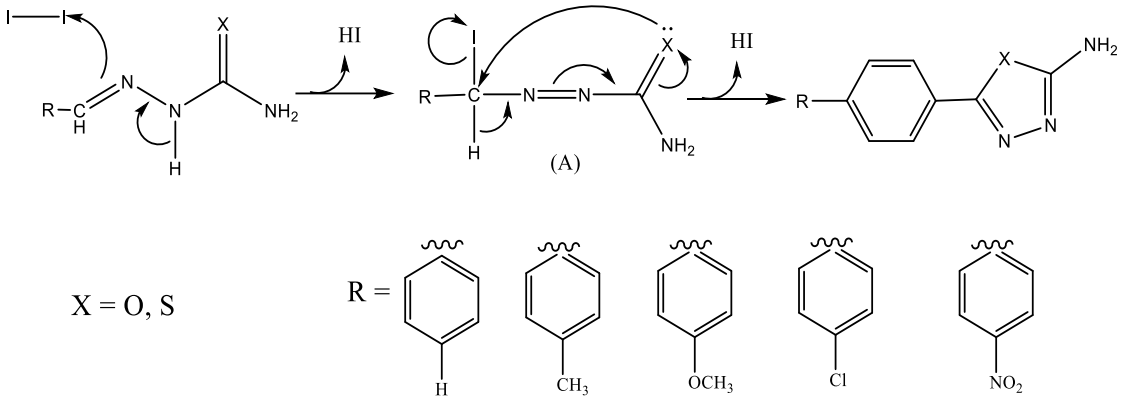

Scheme (3): Mechanism of formation of intermediates (3a-c and 4a-e).[24]

The structure of 1,3,4-oxadiazol derivatives (3a-c) were identified using FT-IR spectroscopy by disappear carbonyl and NH group of compound (1a-c) at (1689.64, 1710.86 and 1691.57 cm^{-1}) and at (3196.05, 3197.98 and 3162.76 cm^{-1}) respectively, and formation of distinctive absorption bands of υ (C=N) for 1,3,4-oxadiazol for compounds (3a-c) at (1650.57, 1658.78, and 1655.59 cm^{-1}), confirmed successful ring closure. And for the 1,3,4-thiadiazol derivatives (4a-e) the disappearance of thioamide and NH group of (2a-e) at υ (1099.43, 1085.92, 1089.78, 1095.24 and 1095.57 cm^{-1}) and (3151.69, 3163.26, 3159.40, 3149.76 and 3127.09 49 cm^{-1}) respectively, and formation of the absorption bands of υ (C=N) for 1,3,4-thiadiazol for compounds (4a-e) at (1632.67, 1637.56, 1638.87, 1631.78, and 1639.49 cm^{-1}) respectively, confirming the completion of cyclization reaction and formation of 1,3,4-thiadiazol derivatives. ^{1}H-NMR Results reveal the peaks of the NH_2 terminal attached to the 1,3,4-oxadiazol ring for the resulted compounds (3a-c) chemical shift equal to δ (6.57, 7.32, 7.18) respectively, and for the 1,3,4-thiadiazol ring for compounds δ (4a-e) equal to (6.89, 7.48, 7.31, 7.39, and 7.72) respectively. ^{13}C-NMR peaks result for compounds (3a-c) for C=N within the 1,3,4-oxadiazol ring show at δ (157.80-164.45), and δ (154.52-170.47) for C=N within the 1,3,4-thiadiazol ring in compounds (4a-e).

Step 3: Mechanism of Formation of Compounds (5a-c, 6a-e):

The final product compound (5a-c, 6a-e) was obtained by a nucleophilic condensation, which involves the reaction of the amino functional group of compounds (3a-c, 4a-e) with the carbonyl of Nabumetone in the presence of glacial acetic acid (GAA) as a catalyst. 1 mL of GAA is used to accelerate the reaction, as shown in Scheme 4 [18].

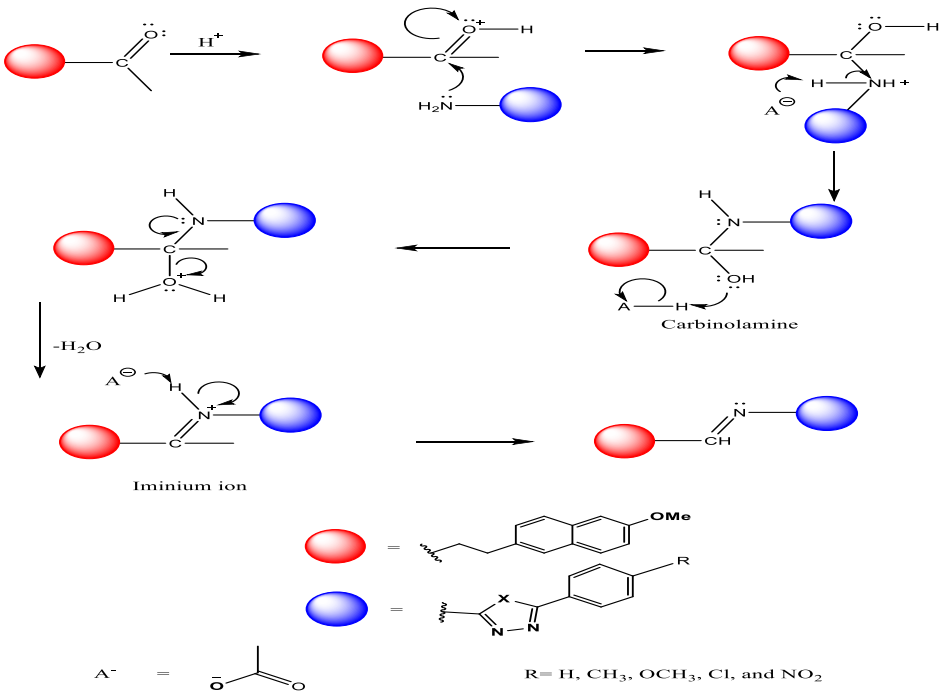

Scheme (4): Showing the mechanism of Schiff base reaction using GAA as a catalyst to form compounds (5a-c, 6a-e). [23, 25]

Identification of final products was done by using FT-IR spectroscopy, which confirm by the formation of imine group υ (C=N) with absorption bands υ at (1607.95, 1625.50, and 1631.78 cm^{-1}) respectively for compounds (5a-c), and the absorption bands for compounds (6a-e) equal to (1600.92, 1602.85, 1604.77, 1598.99 and 1606.70 cm^{-1}) respectively, with disappearance of amine υ (N-H) bands at (3200-3500 cm^{-1}) and carbonyl group of Nabumetone at (1705.07 cm^{-1}).^{1}H-NMR Results show the presence of new methoxy peaks (naphthalene ring side chain) for final compounds ranging from δ (3.82 to 3.86) for compounds (5a-c and 6a-e), also the aromatic region showed signals from the naphthalene ring (multiplets between δ 7.07-7.97), and for the phenyl ring (pattern depending on substituents, e.g. at δ ~8.1 for the nitro-phenyl in compound 6e), also presence of the aliphatic protons (of the butanone moiety of nabumetone side chain) appeared as two triplets around δ 2.78-3.01 ppm, and terminal methyl group around δ (2.08-2.12).^{13}C-NMR peaks were confirmed the result by disappearance of carbonyl peak for Nabumetone at δ (208), and formation of imine (C=N) peak range between δ (169.46-164.38) for the final products, also shifting of terminal methyl group and adjacent (CH_2) group from δ (29.55) and δ (44.60) respectively of Nabumetone to be ranged between δ (20.02-21.47) for terminal methyl group and δ (38.39- 35.42) for adjacent CH_2 group for the final products due to disappearance of carbonyl group and formation of imine group.

3.3 Cytotoxic Activity Assay

The results evaluate the cytotoxicity and the IC_{50} values for eight compounds (5a-c, 6a-e) and the reference drug erlotinib for the A549 lung cancer cell line after 48 hours of exposure. As expected, all compounds displayed increased levels of cytotoxicity with higher concentration levels, which illustrates the dose-response curves for cell death percentages at various concentrations. The

steeper curves for some compounds (like 6b, 6e) demonstrated higher potency for those compounds.

IC_{50}: After 48 hours, Group 6 compounds (6b, 6e) showed IC_{50} values of 40.88 and 30.23, respectively, compared to Group 5 and erlotinib, which had IC_{50} values of 51.35, indicating that they were more potent (Figure 1). This suggests that the 1,3,4-thiadiazole scaffold (Group 6) usually shows higher cytotoxic activity than the 1,3,4-oxadiazole scaffold (Group 5). This means the sulfur atom in the 1,3,4-thiadiazole ring may enable more advantageous interactions with the target protein than the oxygen atom in the 1,3,4-oxadiazole ring. Also, the Substituent Effects alter the activity. In Group 5 (1,3,4-Oxadiazole Derivatives 5a-c), compound 5b, which has a chloro substitution, exhibited a slightly enhanced cytotoxic effect compared to 5a and 5c. Meanwhile, in Group 6 (1,3,4-Thiadiazole Derivatives 6a-e), electron-withdrawing groups, compounds 6b (with chloro substitution) and 6e (with nitro substitution) demonstrated significantly greater IC_{50} values than the other substitutions after 48 hours of treatment. This suggests these structural characteristics may enhance target binding or cellular interaction uptak

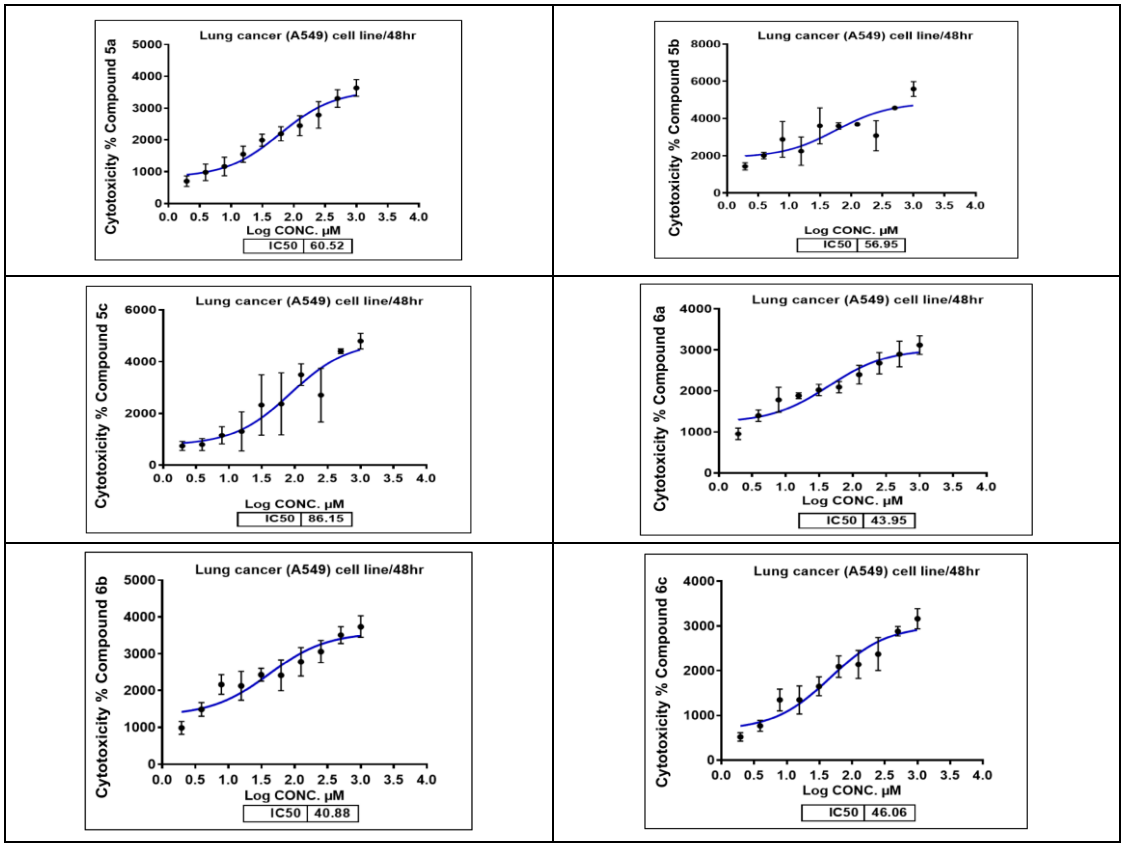

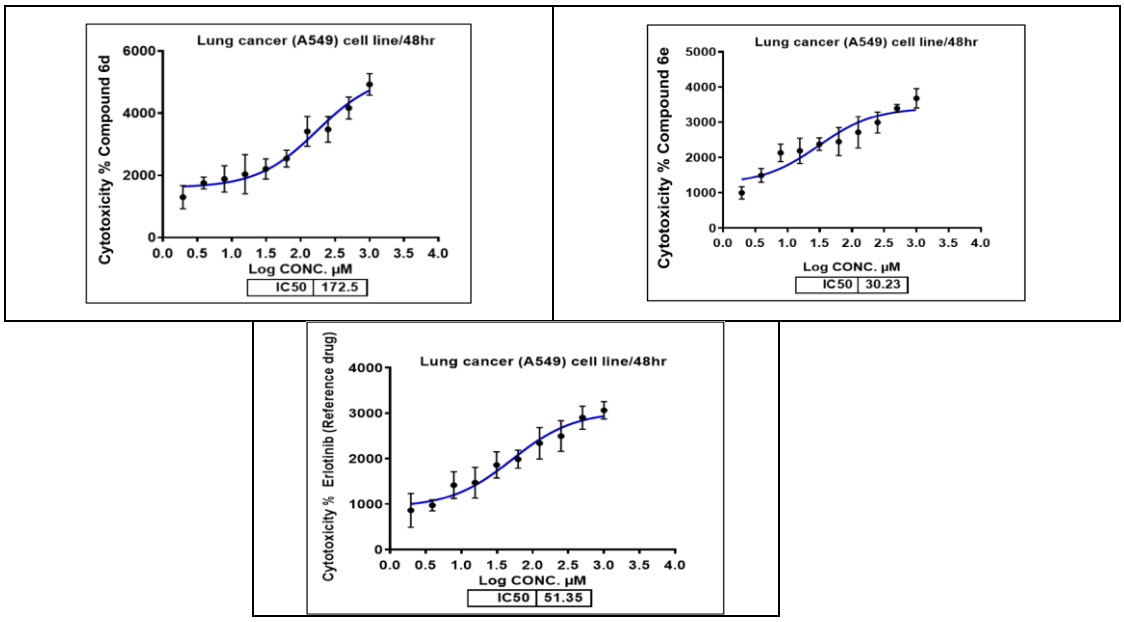

Figure (1): IC_{50} values across different log concentrations (µM) after treating the lung cancer (A549) cell line with all compounds (5a-c, 6a-e), as well as the reference erlotinib (positive control), for 48 hours.

3.1 Statistical Significance and Comparative Analysis

To validate the differences in IC_{50} values among the synthesized compounds and the reference drug, we conducted a statistical analysis using one-way ANOVA followed by multiple comparisons. Figure 2 presents results, with the number of asterisks above the bars indicating statistical significance: * for $p < 0.05$ (significant), ** for $p < 0.01$ (very significant), *** for $p < 0.001$ (highly significant), and **** for $p < 0.0001$ (extremely significant).

The cytotoxicity differences between compounds 6b, 6e, and erlotinib were statistically significant, confirming their superior antiproliferative activity. These findings reinforce the conclusion that 1,3,4-thiadiazole-based derivatives, especially 6b and 6e, exhibit enhanced pharmacological efficacy and deserve further study

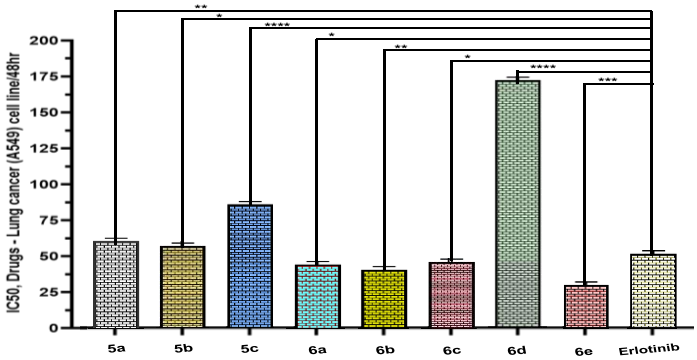

Figure (2): Comparison of IC_{50} values (µM) among all compounds and the reference drug after treatment of the lung cancer (A549) cell line for 48 hours. Asterisks above bars indicate statistical significance compared to erlotinib (p value), where: $p < 0.05$ (*), $p < 0.01$ (**), $p < 0.001$ (***), and $p < 0.0001$ (****).

4. Conclusion

Successfully created and synthesized two novel series of nabumetone-derived Schiff base derivatives that incorporate 1,3,4-oxadiazole (5a-c) or 1,3,4-thiadiazole (6a-e) rings. Molecular Docking results indicated that all compounds bound more strongly to EGFR than erlotinib, with high PLP fitness scores and essential hydrogen bonds with THR830 and THR766.

And by assessed their potential as cytotoxic agents by reducing A549 cell viability. The *in vitro* cytotoxicity assays demonstrated that the compounds can inhibit the growth of NSCLC cells. The thiadiazole-based derivatives (Group 6) were more potent than the oxadiazoles (Group 5) in reducing A549 cell viability, aligning with our design expectations. After 48 hours of treatment, two compounds, 6b (4-chlorobenzylidene thiadiazole) and 6e (4-nitrobenzylidene thiadiazole), achieved IC_{50} values in the low micromolar range (≈30-41 µM), which are lower (better) than that of erlotinib under the same conditions. This enhanced activity of the 1,3,4-thiadiazole series suggests that the sulfur atom in the heterocycle contributes to more favorable than oxygen atom in interactions with the biological target (EGFR) than the oxygen in the oxadiazole ring, consistent with the notion of sulfur's advantageous electronic and binding characteristics. Additionally, a clear structure-activity relationship was observed concerning aromatic substituents.

This study provides substantial proof of concept for utilizing the nabumetone molecular framework to develop new EGFR-targeted anticancer agents. The biological assays are mutually supportive and point to certain compounds (especially 6b and 6e) as promising leads. They could be a foundation for further *in vivo* studies and medicinal chemistry optimization. For example, compound 6e, with its strong electron-withdrawing nitro group, could be further modified to improve solubility or selectivity, or potentially be used as a scaffold for covalent inhibitor development targeting EGFR's cysteine residue. Likewise, 6b's chloro-phenyl group might be amenable to bio-isosteric replacement to enhance its profile.

In conclusion, we have identified a novel set of nabumetone-based Schiff base derivatives that act as promising EGFR inhibitor and demonstrate their cytotoxicity activity via MTT assay. The encouraging findings warrant further investigation, including mechanistic studies to confirm EGFR inhibition at the biochemical level and evaluations in animal models of lung cancer to assess efficacy and safety *in vivo*.

Characterization of Synthesized Compounds

Semicarbazone Intermediates (1a-c)

1a - White powder, yield = 90%, m.p. = 212-214 °C. FTIR (cm^{-1}): 3456, 3287 (N-H/NH_2), 3065 (C-H, Ar), 1689 (C=O), 1601 (C=N), with formula: ($C_8H_9N_3O$).

1b - White crystalline, yield = 83%, m.p. = 240-242 °C. FTIR (cm^{-1}): 3462, 3275 (N-H/H/NH_2), 3069 (C-H, Ar), 1711 (C=O), 1591 (C=N), 825 (C-Cl), with formula: ($C_8H_8ClN_3O$).

1c - White crystalline, yield = 85%, m.p. = 206-208 °C. FTIR (cm^{-1}): 3455, 3286 (N-H/NH_2), 3067 (C-H, Ar), 1692 (C=O), 1611 (C=N), 2829 (C-H, OCH_3), with formula: ($C_9H_{11}N_3O_2$).

Thiosemicarbazone Intermediates (2a-e)

2a - Light grey powder, yield = 87%, m.p. = 170-172 °C. FTIR (cm^{-1}): 3418, 3250 (N-H/NH_2), 3024 (C-H, Ar), 1591 (C=N), 1535 (C=C), 1099 (C=S), with formula: ($C_8H_9N_3S$).

2b - Light brown powder, yield = 84%, m.p. = 205-207 °C. FTIR (cm^{-1}): 3435, 3281 (N-H/H/NH_2), 1599 (C=N), 1524 (C=C), 1086 (C=S), 816 (C-Cl), with formula: ($C_8H_8ClN_3S$).

2c - Grey crystalline solid, yield = 91%, m.p. = 180-182 °C. FTIR (cm^{-1}): 3408, 3281 (N-H/NH_2), 3007 (C-H, Ar), 1601 (C=N), 1535 (C=C), 1090 (C=S), 2837 (C-H, OCH_3), with formula: ($C_9H_{11}N_3OS$).
2d - Light grey powder, yield = 92%, m.p. = 194-196 °C. FTIR (cm^{-1}): 3400, 3256 (N-H/NH_2), 1593 (C=N), 1545 (C=C), 1095 (C=S), 2988 (C-H, CH3), with formula: ($C_9H_{11}N_3S$).
2e - Yellow powder, yield = 90%, m.p. = 245-247 °C. FTIR (cm^{-1}): 3490, 3362 (N-H/H/NH_2), 1582 (C=N), 1508, 1341 (NO_2 asym/sym), 1095 (C=S), with formula: ($C_8H_8N_4O_2S$).

1,3,4-Oxadiazole Intermediates (3a-c)
3a - White powder, yield = 69%, m.p. = 242-244 °C. FTIR (cm^{-1}): 3495, 3320 (N-H), 3038 (C-H, Ar), 1651 (C=N), 1582, 1560 (C=C). ^{1}H-NMR; δ 6.57 (Singlet, 2H, NH2), 7.24-7.28 (Triplet, 1H), 7.46-7.51 (Triplet, 2H), 7.76-7.79 (Doublet, 2H). ^{13}C-NMR; δ 124.82-130.77 (Ar C), 157.80, 164.33 (C=N), with formula: ($C_8H_7N_3O$).
3b - Off-white powder, yield = 75%, m.p. = 263-265 °C. FTIR (cm^{-1}): 3426, 3348 (N-H), 3013 (C-H, Ar), 1659 (C=N), 1570, 1520 (C=C), 829 (C-Cl). ^{1}H-NMR; δ 7.32 (Singlet, 2H, NH_2), 7.50-7.53 (Doublet, 2H), 7.73-7.76 (Doublet, 2H). ^{13}C-NMR; δ 123.64-135.34 (Ar C), 157.01, 164.45 (C=N), with formula: ($C_8H_6ClN_3O$).
3c - Grey crystalline solid, yield = 65%, m.p. = 247-249 °C. FTIR (cm^{-1}): 3417, 3324 (N-H), 3031 (C-H, Ar), 1656 (C=N), 1581 (C=C), 2837 (C-H, OCH_3). ^{1}H-NMR; δ 3.76 (Singlet, 3H, OCH3), 7.00-7.03 (Doublet, 2H), 7.68-7.71 (Doublet, 2H), 7.18 (Singlet, 2H, NH_2). ^{13}C-NMR; δ 55.74 (OCH_3), 115.05, 117.32, 127.24, 161.25 (Ar C), 157.77-163.92 (C=N), with formula: ($C_9H_9N3O_2$).

1,3,4-Thiadiazole Intermediates (4a-e)
4a - White powder, yield = 68%, m.p. = 220-222 °C. FTIR (cm^{-1}): 3345, 3204 (N-H), 1633 (C=N), 1575, 1515 (C=C), 689 (C-S-C). ^{1}H-NMR; δ 6.89 (Singlet, 2H, NH_2), 7.54-7.58 (Triplet, 1H), 7.62-7.66 (Triplet, 2H), 7.72-7.74 (Doublet, 2H). ^{13}C-NMR; δ 126.76-131.49 (Ar C), 156.87, 169.01 (thiadiazole C), with formula: ($C_8H_7N_3S$).
4b - White powder, yield = 72%, m.p. = 225-227 °C. FTIR (cm^{-1}): 1632 (C=N), 1512 (C=C), 690 (C-S), 829 (C-Cl). ^{1}H-NMR; δ 7.48 (Singlet, 2H, NH_2), 7.33-7.37 (Doublet, 2H), 7.72-7.74 (Doublet, 2H). ^{13}C-NMR; δ 128.33-134.43 (Ar C), 155.61, 169.32 (C=N), with formula: ($C_8H_6ClN_3S$).
4c - White crystalline solid, yield = 71%, m.p. = 194-196 °C. FTIR (cm^{-1}): 1639 (C=N), 1584, 1512 (C=C), 2834 (C-H, OCH_3). ^{1}H-NMR; δ 3.75 (Singlet, 3H, OCH_3), 7.31 (Singlet, 2H, NH_2), 6.96-6.99 (Doublet, 2H), 7.64-7.66 (Doublet, 2H). ^{13}C-NMR; δ 55.73 (OCH_3), 114.93, 124.04, 128.27, 160.72 (Ar C), 156.79, 168.38 (thiadiazole C), with formula: ($C_9H_9N_3OS$).
4d - Light grey powder, yield = 61%, m.p. = 200-202 °C. FTIR (cm^{-1}): 3364 (N-H), 1638 (C=N), 1514 (C=C). ^{1}H-NMR; δ 2.28 (Singlet, 3H, CH_3), 7.39 (Singlet, 2H, NH_2), 7.20-7.22 (Doublet, 2H), 7.59-7.62 (Doublet, 2H). ^{13}C-NMR; δ 21 (CH3), 126.68-139.74 (Ar C), 156.99-168.70 (C=N), with formula: ($C_9H_9N_3S$).
4e - Yellow powder, yield = 63%, m.p. = 255-257 °C. FTIR (cm^{-1}): 1639 (C=N), 1595 (C=C), 1508, 1341 (NO_2). ^{1}H-NMR; δ 7.72 (Singlet, 2H), 7.94-7.97 (Doublet, 2H), 8.22-8.24 (Doublet, 2H). ^{13}C-NMR; δ 124.83-147.74 (Ar C), 154.52, 170.47 (C=N), with formula: ($C_8H_6N_4O_2S$).

Final Schiff Base Products 5a-c
5a - Off-white powder. Yield: 45%, m.p.: 190-192 °C. FTIR (cm^{-1}): 3102 (Ar-H), 2962 (C-H, aliphatic), 2832 (C-H, OCH_3), 1664 (C=N, Oxadiazol), 1608 (C=N, imine), 1572 (C=C, Ar). 1H-NMR (DMSO-d_6, 300 MHz); δ 2.08 (Singlet, 3H, CH_3), 2.78-2.82 (Triplet, 2H, CH_2), 2.84-2.88 (Triplet, 2H, CH_2), 3.82 (Singlet, 3H, OCH_3), 7.07-8.04 (Multiplet,

Ar-H). 13C-NMR (75 MHz, DMSO-d6); δ 20.8 (CH_3), 29.5, 35.4 (CH_2), 55.5 (OCH_3), 106.13-157.22 (Ar C), 166.43 (C=N, imine), 162.24, 170.35 (C=N, Oxadiazole). Molecular formula: ($C_{20}H_{18}N_4O_3$).

5b - White powder. Yield: 39%, m.p.: 186-188 °C. FTIR (cm^{-1}): 3064 (Ar-H), 2959 (C-H, aliphatic), 2837 (C-H, OCH_3), 1672 (C=N, Oxadiazol), 1672 (C=N, Imine), 1570 (C=C, Ar), 827 (C-Cl). ^{1}H-NMR; δ 2.12 (Singlet, 3H, CH_3), 2.89-2.91 (Triplet, 2H, CH_2), 2.92-2.95 (triplet, 2H, CH_2), 3.86 (Singlet, 3H, OCH_3), 7.15-8.16 (Multiplet, Ar-H). ^{13}C-NMR; δ 21.47 (CH_3), 30.19, 37.30 (CH_2), 55.51 (OCH_3), 167.98 (C=N, imine), 106.11-157.03 (Ar C), 163.91, 169.21 (C=N, Oxadiazole). Molecular formula: ($C_{20}H_{17}ClN_4O_2$).

5c - Creamy-white powder. Yield: 42%, m.p.: 173-175 °C. FTIR (cm^{-1}): 3072, 3038 (Ar-H), 2997, 2924 (C-H, aliphatic), 2849, 2821 (C-H, OCH_3), 1674 (C=N, Oxadiazol), 1626 (C=N, imine), 1572 (C=C, Ar). ^{1}H-NMR; δ 2.10 (Singlet, 3H, CH_3), 2.79-2.83 (Triplet, 2H, CH_2), 2.84-2.88 (Triplet, 2H, CH_2), 3.84 (Singlet, 3H, Ar-OCH_3), 3.92 (Singlet, 3H, Naph-OCH_3), 6.93-7.99 (Multiplet, Ar-H). ^{13}C-NMR; δ 21.32 (CH_3), 30.16, 37.69 (CH_2), 55.46, 55.70 (OCH_3), 106.09-157.22 (Ar C), 164 (C=N, imine), 163.92, 169.53 (C=N, Oxadiazole). With formula: ($C_{21}H_{20}N_4O_4$).

Final Schiff Base Products 6a-e

6a - Pale brown powder. Yield: 37%, m.p.: 163-165 °C. FTIR (cm^{-1}): 3075, 3040 (Ar-H), 2987, 2909 (C-H, aliphatic), 2824 (C-H, OCH_3), 1661 (C=N, thiadiazol), 1601 (C=N, imine), 1543 (C=C, Ar), 687 (C-S-C). ^{1}H-NMR; δ 2.08 (Singlet, 3H, CH_3), 2.84-2.93 and 2.97-3.01 (Triplet, 4H each, CH_2), 3.83 (Singlet, 3H, OCH_3), 7.08-7.97 (Multiplet, Ar-H). ^{13}C-NMR: δ 20.44 (CH_3), 30.16, 37.51 (CH_2), 55.50 (OCH_3), 106.10-157.19 (Ar C), 169.00 (C=N, imine), 164.45, 170.47 (C=N, thiadiazol), With formula: ($C_{20}H_{18}N_4O_2S$).

6b - Off-white powder. Yield: 36%, m.p.: 175-177 °C. FTIR (cm^{-1}): 3080 (Ar-H), 2994, 2957 (C-H, aliphatic), 2837 (C-H, OCH_3), 1654 (C=N, thiadiazol), 1599 (C=N, imine), 1574, 1544 (C=C, Ar), 710 (C-S), 826 (C-Cl). ^{1}H-NMR; δ 2.12 (Singlet, 3H, CH_3), 2.79-2.88 (Triplet, 4H, each CH_2), 3.86 (Singlet, 3H, OCH_3), 7.07-7.97 (Multiplet, Ar-H). ^{13}C-NMR; δ 20.01 (CH_3), 30.20, 35.46 (CH_2), 55.52 (OCH_3), 106.12-157.22 (Ar C), 169.34 (C=N, imine), 164.34, 170.46 (C=N, thiadiazol), With formula: ($C_{20}H_{17}ClN_4O_2S$).

6c - White powder. Yield: 44%, m.p.: 121-123 °C. FTIR (cm^{-1}): 3059, 3004 (Ar-H), 2932, 2903 (C-H, aliphatic), 2841 (C-H, OCH_3), 1663 (C=N, thiadiazol), 1605 (C=N, imine), 1555, 1510 (C=C, Ar), 716 (C-S). ^{1}H-NMR; δ 2.10 (Singlet, 3H, CH_3), 2.81-2.91 (triplet, 4H, each CH_2), 3.79 (Singlet, 3H, Ar-OCH_3), 3.85 (Singlet, 3H, Naph-OCH_3), 7.00-7.83 (Multiplet, Ar-H). ^{13}C-NMR; δ 20.95 (CH_3), 30.23, 35.42 (CH_2), 55.54, 55.75 (OCH_3), 106.15-160.71 (Ar C), 169.46 (C=N, imine), 164.50, 170.46 (C=N, thiadiazol), With formula: ($C_{21}H_{20}N_4O_4S$).

6d - White crystalline solid. Yield: 35%, m.p.: 188-190 °C. FTIR (cm^{-1}): 3102, 3060 (Ar-H), 2951, 2921 (C-H, aliphatic), 2832 (C-H, OCH_3), 1656 (C=N, thiadiazol),1603 (C=N, imine), 1539 (C=C, Ar), 710 (C-S). ^{1}H-NMR; δ 2.11 (Singlet, 3H, CH_3), 2.34 (Singlet, 3H, Ar-CH_3), 2.81-2.92 (Triplet, 4H, each CH_2), 3.85 (Singlet, 3H, OCH_3), 7.07-7.79 (Multiplet, Ar-H). ^{13}C-NMR; δ 19.29 (CH_3-Ar), 21.29 (CH_3-R), 30.17, 36.45 (CH2), 55.49 (OCH_3), 106.11-157.20 (Ar C), 169.35 (C=N, imine), 163.92, 170.47 (C=N, thiadiazol), With formula: ($C_{21}H_{20}N_4O_2S$).

6e - Yellow powder. Yield: 44%, m.p.: 194-196 °C. FTIR (cm^{-1}): 3103, 3078 (Ar-H), 2994, 2953 (C-H, aliphatic), 2842 (C-H, OCH_3), 1657 (C=N, thiadiazol), 1607 (C=N, imine), 1530, 1356 (NO_2), 1545 (C=C, Ar). ^{1}H-NMR; δ 2.08 (Singlet, 3H, CH_3), 2.79-2.88 (Triplet, 4H, each CH_2), 3.82 (Singlet,

3H, OCH_3), 7.08-8.28 (Multiplet, Ar-H). ^{13}C-NMR; δ 21.55 (CH_3), 30.20, 38.39 (CH_2), 55.52 (OCH_3), 106.13-157.22 (Ar C), 169 (C=N, imine), 164.34, 170.50 (C=N, thiadiazol), With formula: ($C_{20}H_{17}N_5O_4S$).

Reference

1- Boloker G, Wang C, Zhang J. Updated statistics of lung and bronchus cancer in United States (2018). Journal of thoracic disease. 2018;10(3):1158.
2- Siegel RL, Miller KD, Jemal A. Cancer statistics, 2019. CA: a cancer journal for clinicians. 2019;69(1):7-34.
3- Howlader N, Noone A, Krapcho M, Miller D, Brest A, Yu M, et al. SEER cancer statistics review, 1975–2017. National Cancer Institute. 2020;4.
4- K. Bhanumathy K, Balagopal A, Vizeacoumar FS, Vizeacoumar FJ, Freywald A, Giambra V. Protein tyrosine kinases: their roles and their targeting in leukemia. Cancers. 2021;13(2):184.
5- Park K, Tan E-H, O'Byrne K, Zhang L, Boyer M, Mok T, et al. Afatinib versus gefitinib as first-line treatment of patients with EGFR mutation-positive non-small-cell lung cancer (LUX-Lung 7): a phase 2B, open-label, randomised controlled trial. The Lancet Oncology. 2016;17(5):577-89.
6- Shepherd F, Pereira J, Ciuleanu T, Tan E, Hirsh V, Thongprasert S, et al. A randomized placebo-controlled trial of erlotinib in patients with advanced non-small cell lung cancer (NSCLC) following failure of 1st line or 2nd line chemotherapy. A National Cancer Institute of Canada Clinical Trials Group (NCIC CTG) trial. Journal of Clinical Oncology. 2004;22(14_suppl):7022-.
7- Cohen MH, Williams GA, Sridhara R, Chen G, McGuinn Jr WD, Morse D, et al. United States Food and Drug Administration drug approval summary: gefitinib (ZD1839; Iressa) tablets. Clinical Cancer Research. 2004;10(4):1212-8.
8- Blencke S, Zech B, Engkvist O, Greff Z, Őrfi L, Horváth Z, et al. Characterization of a conserved structural determinant controlling protein kinase sensitivity to selective inhibitors. Chemistry & biology. 2004;11(5):691-701.
9- Zeng Y, Yu D, Tian W, Wu F. Resistance mechanisms to osimertinib and emerging therapeutic strategies in nonsmall cell lung cancer. Current opinion in oncology. 2022;34(1):54-65.
10- Kerru N, Gummidi L, Maddila S, Gangu KK, Jonnalagadda SB. A review on recent advances in nitrogen-containing molecules and their biological applications. Molecules. 2020;25(8):1909.
11- Glomb T, Szymankiewicz K, Świątek P. Anti-Cancer Activity of Derivatives of 1,3,4-Oxadiazole. Molecules. 2018;23(12):3361.
12- Ali YS, Mahdi MF, Abd Razik BM, Aburjai T. Design, Molecular Docking, Synthesis, Characterization and Preliminary Evaluation of Novel 1, 3, 4-Oxadiazole Derivatives as Cyclin-Dependent Kinase 2 Inhibitors. Al Mustansiriyah Journal of Pharmaceutical Sciences. 2025;25(1):94-109.
13- Janowska S, Paneth A, Wujec M. Cytotoxic properties of 1, 3, 4-thiadiazole derivatives—A review. Molecules. 2020;25(18):4309.
14- Alawad KM, Mahdi MF, Raauf AM. Molecular Docking study, and In vitro Evaluation of Antitumor Activity of Some New Isoxazoline and Pyrazoline Derivatives of Nabumetone against breast cancer cell line (MCF-7). Al Mustansiriyah Journal of Pharmaceutical Sciences. 2022;22(3):24-34.
15- Stanzione F, Giangreco I, Cole JC. Use of molecular docking computational

tools in drug discovery. Progress in medicinal chemistry. 2021;60:273-343.
16- Coumar MS. Molecular docking for computer-aided drug design: Fundamentals, techniques, resources and applications: Academic Press; 2021.
17- Niu P, Kang J, Tian X, Song L, Liu H, Wu J, et al. Synthesis of 2-amino-1, 3, 4-oxadiazoles and 2-amino-1, 3, 4-thiadiazoles via sequential condensation and I2-mediated oxidative C–O/C–S bond formation. The Journal of organic chemistry. 2015;80(2):1018-24.
18- Dutta B, Das K, Goswami B. Cycloaddition Reaction: Synthesis of 5-Substituted 1, 3, 4-Thiadiazolo [3, 2-a] pyrimidin-6-one. Journal of Chemical Research, Synopses. 1999(1):36-7.
19- Fu Y, Zhao J, Chen Z. Insights into the molecular mechanisms of protein-ligand interactions by molecular docking and molecular dynamics simulation: a case of oligopeptide binding protein. Computational and mathematical methods in medicine. 2018;2018(1):3502514.
20- Patil R, Das S, Stanley A, Yadav L, Sudhakar A, Varma AK. Optimized hydrophobic interactions and hydrogen bonding at the target-ligand interface leads the pathways of drug-designing. PloS one. 2010;5(8):e12029.
21- Gao Q, Liu S, Wu X, Zhang J, Wu A. Direct annulation of hydrazides to 1, 3, 4-oxadiazoles via oxidative C (CO)–C (methyl) bond cleavage of methyl ketones. Organic letters. 2015;17(12):2960-3.
22- Xavier A, Srividhya N. Synthesis and study of Schiff base ligands. IOSR Journal of Applied Chemistry. 2014;7(11):06-15.
23- Abid OH. Preparation and Identification of Novel 1, 3-Oxazepine Derivatives by Cycloaddition Reactions [2+ 5] of Selected Carboxylic Acid Anhydrides with Imines Derived from 4-methyl aniline. Al-Mustansiriyah Journal of Science. 2018;29(2):93-100.
24- Yu W, Huang G, Zhang Y, Liu H, Dong L, Yu X, et al. I2-mediated oxidative C–O bond formation for the synthesis of 1, 3, 4-oxadiazoles from aldehydes and hydrazides. The Journal of Organic Chemistry. 2013;78(20):10337-43.
25- Majeed RHA, Hussein HA, Abdullah MA. Preparation and characterization of novel schiff base derived from 4-nitro benzaldehyde and its cytotoxic activities. International Journal of Molecular and Cellular Medicine. 2022;11(4):285.